

$\chi_b(3P)$ multiplet revisited: Hyperfine mass splitting and radiative transitionsMuhammad Naeem Anwar,^{1,2,3,*} Yu Lu,^{4,†} and Bing-Song Zou^{1,2,‡}¹CAS Key Laboratory of Theoretical Physics, Institute of Theoretical Physics,
Chinese Academy of Sciences, Beijing 100190, China²University of Chinese Academy of Sciences, Beijing 100049, China³Institute for Advanced Simulation, Institut für Kernphysik and Jülich Center for Hadron Physics,
Forschungszentrum Jülich, D-52425 Jülich, Germany⁴Helmholtz-Institut für Strahlen- und Kernphysik and Bethe Center for Theoretical Physics,
Universität Bonn, D-53115 Bonn, Germany

(Received 14 February 2019; published 7 May 2019)

Invoked by the recent CMS observation regarding candidates of the $\chi_b(3P)$ multiplet, we analyze the hyperfine and mass splittings among the $3P$ multiplet in our unquenched quark model studies. The mass difference of χ_{b2} and χ_{b1} in the $3P$ multiplet measured by the CMS Collaboration ($10.6 \pm 0.64 \pm 0.17$ MeV) is very close to our theoretical prediction (12 MeV). Our corresponding mass splitting of χ_{b1} and χ_{b0} enables us to predict more precisely the mass of $\chi_{b0}(3P)$ to be (10490 ± 3) MeV. Moreover, we predict ratios of the radiative decays of $\chi_{bJ}(nP)$ candidates, both in the unquenched quark model and quark potential model. Our predicted relative branching fraction of $\chi_{b0}(3P) \rightarrow \Upsilon(3S)\gamma$ is one order of magnitude smaller than $\chi_{b2}(3P)$; this naturally explains the nonobservation of $\chi_{b0}(3P)$ in the recent CMS search. We hope these results provide useful references for forthcoming experimental searches.

DOI: 10.1103/PhysRevD.99.094005

I. INTRODUCTION

The excited P -wave bottomonia, $\chi_{bJ}(3P)$, are of special interest since they provide a laboratory to test (and model) the nonperturbative spin-spin interactions of heavy quarks. Very recently, the CMS Collaboration observed two candidates of the bottomonium $3P$ multiplet, $\chi_{b1}(3P)$ and $\chi_{b2}(3P)$, through their decays into $\Upsilon(3S)\gamma$ [1]. Their measured masses and mass splitting are

$$\begin{aligned} M[\chi_{b1}(3P)] &= (10513.42 \pm 0.41 \pm 0.18) \text{ MeV}, \\ M[\chi_{b2}(3P)] &= (10524.02 \pm 0.57 \pm 0.18) \text{ MeV}, \\ \Delta m_{21} \equiv m(\chi_{b2}) - m(\chi_{b1}) &= (10.6 \pm 0.64 \pm 0.17) \text{ MeV}. \end{aligned} \quad (1)$$

There are some earlier measurements related to $\chi_{bJ}(3P)$ mass by the ATLAS [2], LHCb [3,4], and D0 collaborations [5]. However, these measurements cannot distinguish between the candidates of the $\chi_{bJ}(3P)$ multiplet. The

*m.anwar@fz-juelich.de
†luyu@hiskp.uni-bonn.de
‡zoubs@itp.ac.cn

Published by the American Physical Society under the terms of the Creative Commons Attribution 4.0 International license. Further distribution of this work must maintain attribution to the author(s) and the published article's title, journal citation, and DOI. Funded by SCOAP³.

recent CMS analysis [1] is a higher-resolution search and hence is able to distinguish between $\chi_{b1}(3P)$ and $\chi_{b2}(3P)$ for the first time.

In this paper, we intend to compare our unquenched quark model studies with this recent measurement and make a more precise prediction for the mass of the other $3P$ bottomonium (χ_{b0}) by incorporating the measured mass splitting. We also make an analysis of the hyperfine splitting of P -wave bottomonia, which enlighten the internal quark structure of the considered bottomonium. In addition, we predict model-independent ratios of radiative decays of $\chi_{bJ}(nP)$ candidates.

Heavy quarkonium states can couple to intermediate heavy mesons through the creation of the light quark-antiquark pair which enlarges the Fock space of the initial state; i.e., the initial state contains multi-quark components. These multi-quark components will change the Hamiltonian of the potential model, causing the mass shift and mixing between states with the same quantum numbers or directly contributing to open channel strong decay if the initial state is above the threshold. These can be summarized as coupled-channel effects (CCEs). When CCEs are combined with the naive quark potential model, one gets the unquenched quark model (UQM). The UQM was considered at least 35 years ago by Törnqvist *et al.* [6–9].

The physical or experimentally observed bottomonium state $|A\rangle$ is expressed in the UQM as

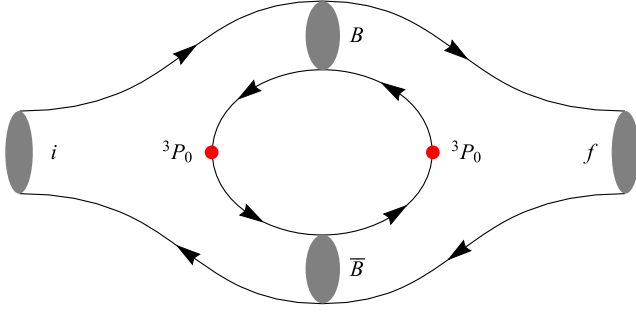


FIG. 1. Sketch of coupled-channel effects in the 3P_0 model. i and f , respectively, denote the initial and final states with the same J^{PC} and $B\bar{B}$ stands for all possible B meson pairs.

$$|A\rangle = c_0|\psi_0\rangle + \sum_{BC} \int d^3p c_{BC}(p)|BC; p\rangle, \quad (2)$$

where c_0 and c_{BC} stand for the normalization constants of the bare state and the BC components, respectively. In this work, B and C refer to bottom and antibottom mesons, and the summation over BC is carried out by including all possible pairs of ground-state bottom mesons. The $|\psi_0\rangle$ is normalized to 1, and $|A\rangle$ is also normalized to 1 if it lies below the $B\bar{B}$ threshold, and $|BC; p\rangle$ is normalized as $\langle BC; p_1|B'C'; p_2\rangle = \delta^3(p_1 - p_2)\delta_{BB'}\delta_{CC'}$, where p is the momentum of the B meson in $|A\rangle$'s rest frame. The full Hamiltonian of the physical state then reads

$$H = H_0 + H_{BC} + H_I, \quad (3)$$

where H_0 is the Hamiltonian of the bare state (see Appendix A for details), $H_{BC}|BC; p\rangle = E_{BC}|BC; p\rangle$ with $E_{BC} = \sqrt{m_B^2 + p^2} + \sqrt{m_C^2 + p^2}$ is the energy of the continuum state (interaction between B and C is neglected, and the transition between one continuum to another is restricted), and H_I is the interaction Hamiltonian which mixes the bare state with the continuum. Since each quark pair creation model generates its own vertex functions that in turn lead to specific real parts of hadronic loops, see Ref. [10] for related remarks.

Here, for the bare-continuum mixing, we adopt the widely used 3P_0 model [11]. In this model, the generated quark pairs have vacuum quantum numbers $J^{PC} = 0^{++}$, which in spectroscopical notation ${}^{2S+1}L_J$ equals 3P_0 . A sketch of the 3P_0 model induced mixing is shown in Fig. 1. The interaction Hamiltonian can be expressed as

$$H_I = 2m_q\gamma \int d^3x \bar{\psi}_q \psi_q, \quad (4)$$

where m_q is the produced quark mass and γ is the dimensionless coupling constant. The ψ_q ($\bar{\psi}_q$) is the spinor field to generate the antiquark (quark). Since the probability to generate heavier quarks is suppressed, we use the effective strength $\gamma_s = \frac{m_q}{m_s}\gamma$ in the following calculation,

where $m_q = m_u = m_d$ is the constituent quark mass of the up (or down) quark and m_s is the strange quark mass.

The mass shift caused by the BC components and the probabilities of the $b\bar{b}$ core are obtained after solving the Schrödinger equation with the full Hamiltonian H . They are expressed as

$$\Delta M := M - M_0 = \sum_{BC} \int d^3p \frac{|\langle BC; p|H_I|\psi_0\rangle|^2}{M - E_{BC} - i\epsilon}, \quad (5)$$

$$P_{b\bar{b}} := |c_0|^2 = \left(1 + \sum_{BCLS} \int d^3p \frac{p^2 \langle BC; p|H_I|\psi_0\rangle|^2}{(M - E_{BC})^2}\right)^{-1}, \quad (6)$$

where M and M_0 are the eigenvalues of the full (H) and quenched/bare Hamiltonian (H_0), respectively. See Appendix B or Refs. [12,13] for the derivation of above relations and UQM calculation details. Numerical values of ΔM and $P_{b\bar{b}}$ of every coupled channel for the bottomonia below the $B\bar{B}$ threshold are given in Table I, which will be used in the following discussions.

II. MASS SPLITTING AND $\chi_{b0}(3P)$

After the recent CMS observation [1] of $\chi_{b1}(3P)$ and $\chi_{b2}(3P)$, $\chi_{b0}(3P)$ is now the only missing candidate in spin-triplet $3P$ bottomonium. With the reference of observed mass splitting of $1P$, $2P$, and $3P$ multiplets, one can predict the mass of $\chi_{b0}(3P)$. It requires a constraint that the mass splittings for the $1P$, $2P$ and $3P$ multiplets should be the same [14].

Triggered by the above-mentioned experimental search, we analyze our UQM studies regarding the bottomonium spectrum [12,15]. We notice that the measured mass splitting between $\chi_{b2}(3P)$ and $\chi_{b1}(3P)$ is $(10.6 \pm 0.64 \pm 0.17)$ MeV, which differs only by 1 MeV from our UQM prediction¹ [12]. Our prediction for the mass splitting of $\chi_{b1}(3P)$ and $\chi_{b0}(3P)$ is 23 MeV; see Table II. With the reference of the observed masses of the other two candidates of spin-triplet $3P$ bottomonium, this mass splitting helps us to predict precisely the mass of unknown $\chi_{b0}(3P)$ to be

$$M[\chi_{b0}(3P)] = (10490 \pm 3) \text{ MeV}. \quad (7)$$

The uncertainty in the above prediction is calculated by taking the same percentage error [of $\mathcal{O}(10\%)$] in our mass splittings which we observed from the CMS measurement [1]. Our mass predictions respect the conventional pattern of splitting and support the standard mass hierarchy, where we have $M(\chi_{b2}) > M(\chi_{b1}) > M(\chi_{b0})$, which is in line with the CMS measurement [1]. A comparison of our UQM

¹In the quenched limit, where the sea quark fluctuations are neglected, this difference becomes six times larger.

TABLE I. The mass shift (in MeV) and probability (in percent) of every coupled channel for the bottomonia below the $B\bar{B}$ threshold. Note that, since $h_b(3P)$ has no coupling to $B\bar{B}$, even though $h_b(3P)$ is above the $B\bar{B}$ threshold, the probability is still well defined. However, $\chi_{b2}(3P)$ couples to the $B\bar{B}$ channel and lies above this threshold, causing difficulty to the renormalization of the wave function. We make the assumption that the renormalization caused by the $B\bar{B}$ channel can be discarded; see Sec. IV for related discussions.

Initial states	$B\bar{B}$		$B\bar{B}^* + \text{H.c.}$		$B^*\bar{B}^*$		$B_s\bar{B}_s$		$B_s\bar{B}_s^* + \text{H.c.}$		$B_s^*\bar{B}_s^*$		Total	
	$-\Delta M$	$P_{b\bar{b}}$	$-\Delta M$	$P_{b\bar{b}}$	$-\Delta M$	$P_{b\bar{b}}$	$-\Delta M$	$P_{b\bar{b}}$	$-\Delta M$	$P_{b\bar{b}}$	$-\Delta M$	$P_{b\bar{b}}$	$-\Delta M$	$P_{b\bar{b}}(\%)$
$\eta_b(1S)$	0	0	7.8	0.45	7.6	0.43	0	0	3.3	0.17	3.3	0.16	22.0	98.79
$\eta_b(2S)$	0	0	16.5	1.81	15.7	1.62	0	0	5.2	0.43	5.0	0.4	42.4	95.74
$\eta_b(3S)$	0	0	24.5	5.01	22.3	3.98	0	0	5.4	0.63	5.1	0.55	57.4	89.83
$\Upsilon(1S)$	1.4	0.09	5.4	0.33	9.2	0.54	0.6	0.03	2.3	0.12	3.9	0.2	22.8	98.69
$\Upsilon(2S)$	3.0	0.37	11.4	1.29	18.9	2.02	0.9	0.08	3.5	0.31	5.9	0.49	43.8	95.44
$\Upsilon(3S)$	4.8	1.25	17.2	3.71	27.1	5.07	1.0	0.13	3.7	0.45	6.1	0.67	60.0	88.71
$h_b(1P)$	0	0	13.5	1.22	13.0	1.12	0	0	4.8	0.35	4.6	0.33	35.8	96.99
$h_b(2P)$	0	0	21.9	3.51	20.3	2.96	0	0	5.6	0.59	5.3	0.52	53.1	92.43
$h_b(3P)$	0	0	38.0	19.75	29.5	9.04	0	0	5.4	0.67	5.0	0.54	77.9	70.0
$\chi_{b0}(1P)$	4.1	0.45	0	0	21.4	1.74	1.3	0.11	0	0	7.8	0.52	34.6	97.18
$\chi_{b0}(2P)$	9.3	1.85	0	0	31.1	4.13	2.1	0.26	0	0	8.4	0.77	50.9	92.98
$\chi_{b0}(3P)$	25.5	34.08	0	0	40.7	8.07	2.3	0.31	0	0	7.6	0.62	76.1	56.92
$\chi_{b1}(1P)$	0	0	10.8	1.03	15.5	1.27	0	0	3.7	0.28	5.6	0.38	35.5	97.03
$\chi_{b1}(2P)$	0	0	19.7	3.38	22.1	3.0	0	0	4.8	0.53	6.0	0.56	52.6	92.53
$\chi_{b1}(3P)$	0	0	37.4	21.9	29.7	7.54	0	0	4.8	0.64	5.4	0.54	77.4	69.38
$\chi_{b2}(1P)$	3.4	0.31	9.8	0.85	13.6	1.24	1.2	0.09	3.5	0.25	4.7	0.35	36.4	96.91
$\chi_{b2}(2P)$	5.3	0.89	14.6	2.23	23.2	3.62	1.3	0.15	3.8	0.39	5.8	0.6	54.1	92.13
$\chi_{b2}(3P)$	12.3	...	23.3	12.50	36.2	16.34	1.3	0.23	3.6	0.53	5.6	0.82	82.2	69.57

TABLE II. Mass splitting (in MeV) of $3P$ -wave bottomonia in our UQM [12], Godfrey-Isgur (GI) model [16], modified GI model [17], and constituent quark model (CQM) [18]. The later three models are regarded as quenched quark models.

Mass splitting	Our UQM [12]	GI [16]	Modified GI [17]	CQM [18]	Experiment [1]
$\chi_{b1}(3P) - \chi_{b0}(3P)$	23	16	14	13	...
$\chi_{b2}(3P) - \chi_{b1}(3P)$	12	12	12	9	$(10.6 \pm 0.64 \pm 0.17)$

mass splittings with other quenched quark model predictions is given in Table II.

III. HYPERFINE SPLITTING IN UQM

It is more informative if we study the mass splitting in a multiplet instead of the total mass shift caused by the intermediate meson loop. For the states quite below the threshold, there is an interesting phenomenon [19]: the magnitude of the mass splitting is suppressed by the probability of the bottomonium core, $P_{b\bar{b}}$, if we turn on the meson loop.

There is also a pictorial explanation for this. In potential model, the mass splitting δM_0 originates from the fine splitting Hamiltonian H_I . Up to the first-order perturbation, we have $\delta M_0 = \langle \psi | H_I | \psi \rangle$, where ψ is the two-body wave function in the quenched potential model. Since one of the coupled-channel effects is the wave function renormalization, $\langle \psi | \psi \rangle = P_{b\bar{b}} < 1$, one would simply expect the δM_0 to be suppressed by this probability.

Moreover, due to the closeness of the spectrum of a multiplet, we expect that the $P_{b\bar{b}}$ of the states in the same multiplet are nearly the same, i.e., δM_0 are all suppressed by a same quantity, leaving the relation

$$\delta M_P \equiv \frac{1}{9} [M(\chi_{b0}) + 3 \cdot M(\chi_{b1}) + 5 \cdot M(\chi_{b2})] - M(h_b) = 0 \tag{8}$$

intact, even if the coupled-channel effects are turned on. In our calculation, however, due to the finite size of the constituent quark, which is reflected by the smeared delta term, $\tilde{\delta}(r)$, instead of the true Dirac term² in the spin dependent potential

²Such a *smearing* of the Dirac delta term incorporating the contact spin-spin interaction with a finite range $1/\sigma$ is essential to regularize the delta function [20].

TABLE III. Hyperfine splitting (δM_P in MeV) for the P -wave bottomonia. The second to fourth columns are our unquenched quark model prediction, contribution from the coupled-channel effects, and experimental results, respectively. The contribution from coupled-channel effects can be obtained by replacing the mass of $\chi_{bJ}(nP)$ by their mass shift ΔM . Note that our results of M_0 violate Eq. (8) a bit due to the finite size of the constituent quark, as discussed in the text.

Multiplet	UQM prediction	CCEs contribution	Experiment [21]
1P	1.17	0.06	0.57(88)
2P	1.38	0.19	0.44(1.31)
3P	-0.39	2.08	...

$$V_s(r) = \frac{1}{m_b^2} \left[\left(\frac{2\alpha_s}{r^3} - \frac{\lambda}{2r} \right) \mathbf{L} \cdot \mathbf{S} + \frac{32\pi\alpha_s}{9} \tilde{\delta}(r) \mathbf{S}_b \cdot \mathbf{S}_{\bar{b}} + \frac{4\alpha_s}{r^3} \left(\frac{\mathbf{S}_b \cdot \mathbf{S}_{\bar{b}}}{3} + \frac{(\mathbf{S}_b \cdot \mathbf{r})(\mathbf{S}_{\bar{b}} \cdot \mathbf{r})}{r^2} \right) \right],$$

$$\tilde{\delta}(r) \equiv \left(\frac{\sigma}{\sqrt{\pi}} \right)^3 e^{-\sigma^2 r^2}, \quad (9)$$

where α_s and λ are strengths of the color Coulomb and linear confinement potentials, respectively, and σ is related to the width of Gaussian smeared function, the δM_P relation of Eq. (8) is already violated a little bit under the potential model, which can be seen from Table III (second column), in which we also include the corresponding experimental values. We can also extract the threshold effects by taking the mass shift ΔM instead of M in δM_P calculations. The δM_P values obtained in this way are also given in Table III (third column).

We can see from Table I that, although the mass shift for the P -wave multiplets is around 50 MeV, the modification of Eq. (8) is not very large, except $\delta M_P(3P)$, which is far larger than $\delta M_P(2P)$ and $\delta M_P(1P)$. A feature worth mentioning here is the hierarchy of these hyperfine splittings originating from the CCEs (third column of Table III), viz.,

$$\delta M_P(3P) > \delta M_P(2P) > \delta M_P(1P), \quad (10)$$

which highlights that the coupled-channel effects bring meson masses closer together with respect to their bare values [19].

For the P -wave states, no matter whether the threshold effects are considered or not, h_b is not affected by the fine interaction, i.e. the $\delta M = 0$. Hence, the χ_{bJ} 's mass splitting are purely due to the $P_{b\bar{b}}$ of each χ_{bJ} . Therefore, the weighted probability of the bottomonium core, $\tilde{P}_{b\bar{b}}$, for $\chi_{bJ}(nP)$ multiplets is simply defined as $\tilde{P}_{b\bar{b}} = P_{b\bar{b}}(\chi_{bJ})$. The weighted average probability for the S -wave bottomonia is discussed in Appendix C. From Table IV, we can see that, although the ($\tilde{P}_{b\bar{b}} \times \delta M_0$) and δM originate differently (one from the potential model and the other purely from the coupled-channel effects), they are approximately equal to each other. The only large deviation comes from $\chi_{bJ}(3P)$.

As explained above, this overall suppression is based on the assumption that the $\tilde{P}_{b\bar{b}}$ is the same (or approximately the same) for a multiplet. Indeed, from Table I, we can see that this is a quite reasonable assumption for the states which are far below the threshold. But for the $\chi_{b0}(3P)$, the $\tilde{P}_{b\bar{b}}$ is quite different from that of $\chi_{b1}(3P)$, so this overall suppression does not make sense anymore. As a

TABLE IV. The mass splitting (in MeV) in a same (n, L) multiplet, where δM_0 , δM , and δM_{Exp} represent the mass splitting in potential model, coupled-channel model, and experiment, respectively. The $\tilde{P}_{b\bar{b}}$ (in percent) is the weighted average of the probability, which for the P and S waves is $\tilde{P}_{b\bar{b}} = P_{b\bar{b}}(\chi_{bJ})$ and $\tilde{P}_{b\bar{b}} = \frac{1}{4}P_{b\bar{b}}(\Upsilon) + \frac{3}{4}P_{b\bar{b}}(\eta_b)$, respectively. The details of the mass splitting are given in Appendix C, and the absolute probabilities $P_{b\bar{b}}$ are given in Table I. GEM and SHO stand for the Gaussian expansion method [22] and simple harmonic oscillator approximation, respectively, to fit the numerical wave functions.

Channels	δM_0	$\tilde{P}_{b\bar{b}}$	$(\tilde{P}_{b\bar{b}} \times \delta M_0)$	δM	$\tilde{P}_{b\bar{b}}$	$(\tilde{P}_{b\bar{b}} \times \delta M_0)$	δM	δM_{Exp}
		GEM		SHO				
$\Upsilon(1S) - \eta_b(1S)$	65.5	98.7	64.7	64.7	98.7	64.7	64.7	62.3
$\Upsilon(2S) - \eta_b(2S)$	30.7	95.5	29.3	29.4	95.9	29.4	29.5	24.3
$\Upsilon(3S) - \eta_b(3S)$	23.4	89.0	20.8	20.7	91.1	21.3	21.3	...
$\chi_{b0}(1P) - h_b(1P)$	-35.6	97.2	-34.6	-34.5	97.1	-34.6	-34.4	-39.9
$\chi_{b1}(1P) - h_b(1P)$	-6.3	97.0	-6.1	-6.0	97.0	-6.1	-6.0	-6.5
$\chi_{b2}(1P) - h_b(1P)$	13.2	96.9	12.8	12.6	96.8	12.8	12.7	12.9
$\chi_{b0}(2P) - h_b(2P)$	-31.2	93.0	-29.0	-28.9	93.4	-29.2	-29.1	-27.3
$\chi_{b1}(2P) - h_b(2P)$	-5.4	92.5	-5.0	-4.9	93.0	-5.0	-5.0	-4.3
$\chi_{b2}(2P) - h_b(2P)$	12.2	92.1	11.2	11.2	92.7	11.3	11.2	8.8
$\chi_{b0}(3P) - h_b(3P)$	-29.2	56.9	-16.6	-27.5	54.3	-15.8	-28.3	...
$\chi_{b1}(3P) - h_b(3P)$	-5.0	69.4	-3.5	-4.5	72.5	-3.6	-4.6	...
$\chi_{b2}(3P) - h_b(3P)$	11.9	7.5	7.7	...

consequence, one should expect a relatively large deviation from the δM_P relation, as can be seen from $\delta M_P(3P)$ in Table III.

The reason for this peculiar $\tilde{P}_{b\bar{b}}$ is that, even though the mass of $h_b(3P)$ and $\chi_{b1}(3P)$ is larger than the $\chi_{b0}(3P)$, they do not couple to the channel $B\bar{B}$, and the next open channel $B\bar{B}^*$ is somewhat farther from them. A net effect is that the $\tilde{P}_{b\bar{b}}$ of $\chi_{b1}(3P)$ is larger than that of $\chi_{b0}(3P)$, breaking the $\tilde{P}_{b\bar{b}}$ closeness assumption. This strong coupling of $\chi_{b0}(3P)$ to $B\bar{B}$ is also reflected by the large mass shift caused by $B\bar{B}$, which can be seen in Table I. The observed mismatch between $(\tilde{P}_{b\bar{b}} \times \delta M_0)$ and δM for the $\chi_{bJ}(3P)$ multiplet is a smoking gun of the threshold effects which are beyond the quark potential model.

Recently, Lebed and Swanson also pointed out the remarkable importance of the P -wave heavy quarkonia [23]. For $1P$ and $2P$ charmonia, the hyperfine splitting is found to be astonishingly small. They referred it as *ultrafine splitting* [which is Eq. (8) of this paper] and argued that it can be used to delve the exoticness of the observed structure in the given multiplet [24]. According to their analysis [23], the quantity $\delta M_{n,L=1,2,3,\dots}$ is found to be very small for any radial excitation n , both for the $b\bar{b}$ and $c\bar{c}$ sectors. The obtained constraint on the $\delta M_{n,L}$ value is

$$\delta M_{n,L=0,1,2,\dots} \ll \Lambda_{\text{QCD}}. \quad (11)$$

This conclusion follows from several theoretical formalisms which do not consider coupled-channel effects or long-distance light-quark contributions in terms of intermediate meson-meson coupling to bare quarkonium states. As discussed above, the operators corresponding to hyperfine splitting involve spin-spin interactions which are suppressed by $1/m_Q^2$, the standard expansion parameter for the heavy quarkonium, where m_Q is the mass of the heavy quark. According to our point of view, the above upper limit is very large for the hyperfine splitting of P -wave bottomonia; see Table III for experimental corroboration. The tighter constraint could be

$$\delta M_{n,L=1,2,3,\dots} \lesssim \frac{\Lambda_{\text{QCD}}^3}{m_Q^2}. \quad (12)$$

Quantitatively, the P -wave excitation for the bottomonium is equal to Λ_{QCD} , which describes the emergence of the dynamical QCD scale in the above relation. The $\delta M_{n,L}$ for the bottomonia with $L = 1$ is expected to be of $\mathcal{O}(1 \text{ MeV})$, which can be verified from our analysis of Table III.

The reason why $\delta M_{n,L=1,2,3,\dots}$ is exactly zero in the quark model is a consequence of the pure delta function nature of the $\mathbf{S}_b \cdot \mathbf{S}_{\bar{b}}$ term of Eq. (9), which is a perturbative one gluon exchange effect. The nonperturbative effects can make an additional contribution to this term, so that it is no longer a pure delta function. This gives rise to introducing

the smearing of the delta function in the quark models [20,23]. However, one could use different nonperturbative forms for the spin-spin operator that contributes to the hyperfine splitting. For instance, the hyperfine splitting computed at next-to-next-to-next-to-leading order [25] in nonrelativistic QCD (NRQCD) [26,27] is

$$\delta M_{n,L=1} = \frac{m_b C_F^4 \alpha_s^5}{432\pi(n+1)^3} (4n_l - N_c), \quad (13)$$

where C_F is the color factor of bottomonium, n_l being the number of light fermion species appearing in loop corrections, and N_c being the number of colors in QCD. The computed $\delta M_{n,L=1}$ values using NRQCD for the bottomonium [with $m_b = 4.5 \text{ GeV}$ and $\alpha_s(m_b) = 0.2$] are $\delta M_{1P} = 3.77 \text{ keV}$, $\delta M_{2P} = 1.12 \text{ keV}$, and $\delta M_{3P} = 0.47 \text{ keV}$ [23]. The remarkable smallness of these values strengthens the constraint on the $\delta M_{n,L=1,2,3,\dots}$ values presented in Eq. (12). However, these NRQCD predictions are much smaller as compared to our UQM predictions and corresponding experimental values; see Table III. In conclusion, whatever the nonperturbative form for the spin-spin operator is used, the $\delta M_{n,L=1}$ should be very small, hence satisfying the relation of Eq. (12) quantitatively.

IV. RADIATIVE TRANSITIONS

Radiative transitions of higher bottomonia are of considerable interest since they can shed light on their internal structure and provide one of the few pathways between different $b\bar{b}$ multiplets. Particularly, for those states which cannot directly produce at e^+e^- colliders (such as P -wave bottomonia), the radiative transitions serve as an elegant probe to explore such systems. In the quark model, the electric dipole ($E1$) transitions can be expressed as [28,29]

$$\Gamma(n^{2S+1}L_J \rightarrow n'^{2S'+1}L'_{J'} + \gamma) = \frac{4}{3} C_{fi} \delta_{SS'} e_b^2 \alpha |\langle \psi_f | r | \psi_i \rangle|^2 E_\gamma^3, \quad (14)$$

where $e_b = -\frac{1}{3}$ is the b -quark charge, α is the fine structure constant, and E_γ denotes the energy of the emitted photon. The spatial matrix elements $\langle \psi_f | r | \psi_i \rangle$ involve the initial and final radial wave functions, and C_{fi} are the angular matrix elements. They are represented as

$$\langle \psi_f | r | \psi_i \rangle = \int_0^\infty R_f(r) R_i(r) r^3 dr, \quad (15)$$

$$C_{fi} = \max(L, L') (2J' + 1) \begin{Bmatrix} L' & J' & S \\ J & L & 1 \end{Bmatrix}^2. \quad (16)$$

The matrix elements $\langle \psi_f | r | \psi_i \rangle$ are obtained numerically; for further details, we refer the reader to Refs. [12,30]. From Eq. (15), we know that the value of the decay width

depends on the details of the wave functions, which are highly model dependent. However, we intend to make predictions in a more model-independent way. A model-independent prediction can be achieved by focusing on the following decay ratios:

$$\Gamma(\chi_{bJ}(mP) \rightarrow \Upsilon(nS) + \gamma) / \Gamma(\chi_{b0}(mP) \rightarrow \Upsilon(nS) + \gamma). \quad (17)$$

Since, in the quark model, the spatial wave function is the same for the states in the same multiplet. Therefore, the above ratio can eliminate the wave function dependence—and hence model dependence, too. From the above discussion, we know that the meson loop renormalizes the bottomonium wave function. When the channel is above the corresponding open-bottom threshold (such as $B\bar{B}$ here), the wave function cannot be normalized to 1; this is still an open problem (see, e.g., Ref. [31]). On the other hand, the $B\bar{B}$ loop is still there and has some CCEs (such as mass renormalization). We make the assumption that for the states above threshold [such as $\chi_{b2}(3P)$ here], these open channels contribute equally to the wave functions of all $\chi_{bJ}(3P)$ states. In practice, this is a reasonable assumption, since we can see this from Table I, the probability of $B\bar{B}$ is vanishingly small (0.31% and 0.89%, less than 1%) for both $\chi_{b0}(3P)$ and $\chi_{b1}(3P)$.

With the latest CMS data [1] and the $P_{b\bar{b}}$ in Table I, our predictions of radiative decay ratios are listed in Table V. From Table I, one can see that the small $P_{b\bar{b}}[\chi_{b0}(3P)]$ make the ratios in the last three rows notably larger than that of the potential model predictions, a peculiar feature of coupled-channel effects which can be tested in the upcoming experiments.

Another result worth noting from Table V is the relative size of the ratios for $\chi_{b0}(3P)$, which from the coupled-channel calculations is roughly 1:6:12. This reflects that the $\chi_{b0}(3P)$ has a negligible radiative decay branching fraction with comparison to $\chi_{b1}(3P)$ and $\chi_{b2}(3P)$. Compared with the potential model, the suppression of the $\chi_{b0}(3P)$'s radiative width in the UQM is more consistent with the nonobservation of the $\chi_{b0}(3P)$ in the recent

CMS search of $\chi_{bJ}(3P) \rightarrow \Upsilon(3S)\gamma$ [1]. This indicates that our UQM predictions are more reliable than the naive quark potential models.

V. CONCLUSIONS

The recent CMS study successfully distinguishes $\chi_{b1}(3P)$ and $\chi_{b2}(3P)$ for the first time and measures their mass splitting, which differs only 1 MeV from our unquenched quark model predictions. This measurement gives us confidence to predict the mass of the lowest candidate of the $3P$ multiplet to be $M[\chi_{b0}(3P)] = (10490 \pm 3)$ MeV, based on our unquenched quark model results of the mass splittings of this multiplet. We also analyze the hyperfine splittings of P -wave bottomonia up to $n = 3$ in the framework of UQM and put a constraint on them based on recent experimental corroboration. No matter which nonperturbative form for the spin-spin operator is used, the hyperfine splitting for the P -wave bottomonia should be very small. This analysis leads us to conclude that the coupled-channel effects play a crucial role in understanding the higher bottomonia close to open-flavor thresholds.

At last, we predict here to some extent model-independent ratios of the radiative decays of $\chi_{bJ}(nP)$ candidates. An observation worth mentioning is that the coupled-channel effects can enhance the radiative decay ratios of $\chi_{bJ}(3P)$ as compared to the naive potential model predictions. The relative branching fraction of $\chi_{b0}(3P) \rightarrow \Upsilon(3S)\gamma$ is negligible as compared to the other candidates of this multiplet, which naturally explains its nonobservation in the recent CMS search.

We hope the above highlighted features of the coupled-channel model provide useful references for the understanding of higher P -wave bottomonia and can be explored in ongoing and future experiments.

ACKNOWLEDGMENTS

We are grateful to Timothy J. Burns, Feng-Kun Guo, Richard F. Lebed, and Thomas Mehen for useful discussions and suggestions and to Christoph Hanhart for careful reading of this manuscript and valuable remarks. M. N. A. extends a heartfelt thanks to his wife Anila Yousaf, and Y. L. is thankful to his wife Xiaolei Hua, for their continuous moral support. This work is supported in part by the DFG (Grant No. TRR110) and the NSFC (Grant No. 11621131001) through the funds provided to the Sino-German CRC 110 ‘‘Symmetries and the Emergence of Structure in QCD’’ and by the CAS-TWAS President’s Fellowship for International Ph.D. Students.

APPENDIX A: BARE HAMILTONIAN

Bare states are obtained by solving the Schrödinger equation with the well-known Cornell potential [32,33], which incorporates a spin-independent color Coulomb plus

TABLE V. Prediction for the ratios $\Gamma(\chi_{bJ}(mP) \rightarrow \Upsilon(nS) + \gamma) / \Gamma(\chi_{b0}(mP) \rightarrow \Upsilon(nS) + \gamma)$. The order of previous ratios can be read as $\chi_{b0}:\chi_{b1}:\chi_{b2}$. For potential model calculations, the parameters and quenched Hamiltonian are the same as Ref. [12].

Decay channel	Potential model	Unquenched quark model
$\chi_{bJ}(1P) \rightarrow \Upsilon(1S) + \gamma$	1:3.80:7.20	1:3.79:7.18
$\chi_{bJ}(2P) \rightarrow \Upsilon(1S) + \gamma$	1:3.27:5.71	1:3.25:5.65
$\chi_{bJ}(2P) \rightarrow \Upsilon(2S) + \gamma$	1:4.09:8.02	1:4.07:7.95
$\chi_{bJ}(3P) \rightarrow \Upsilon(1S) + \gamma$	1:3.20:5.49	1:3.90:6.71
$\chi_{bJ}(3P) \rightarrow \Upsilon(2S) + \gamma$	1:3.46:6.15	1:4.22:7.51
$\chi_{bJ}(3P) \rightarrow \Upsilon(3S) + \gamma$	1:4.83:9.77	1:5.89:11.9

linear confined (scalar) potential. In the quenched limit, the potential can be written as

$$V(r) = -\frac{4\alpha}{3r} + \lambda r + c, \quad (\text{A1})$$

where α , λ , and c stand for the strength of color Coulomb potential, the strength of linear confinement, and mass renormalization, respectively. The hyperfine and fine structures are generated by the spin-dependent interactions

$$V_s(r) = \frac{1}{m_b^2} \left[\left(\frac{2\alpha_s}{r^3} - \frac{\lambda}{2r} \right) \mathbf{L} \cdot \mathbf{S} + \frac{32\pi\alpha_s}{9} \tilde{\delta}(r) \mathbf{S}_b \cdot \mathbf{S}_{\bar{b}} + \frac{4\alpha_s}{r^3} \left(\frac{\mathbf{S}_b \cdot \mathbf{S}_{\bar{b}}}{3} + \frac{(\mathbf{S}_b \cdot \mathbf{r})(\mathbf{S}_{\bar{b}} \cdot \mathbf{r})}{r^2} \right) \right], \quad (\text{A2})$$

where \mathbf{L} denotes the relative orbital angular momentum, $\mathbf{S} = \mathbf{S}_b + \mathbf{S}_{\bar{b}}$ is the total spin of the charm quark pairs, and m_b is the bottom quark mass. The smeared $\tilde{\delta}(r)$ function can be read from Eq. (9) or Refs. [20,34]. These spin-dependent terms are treated as perturbations.

The Hamiltonian of the Schrödinger equation in the quenched limit is represented as

$$H_0 = 2m_b + \frac{p^2}{m_b} + V(r) + V_s(r). \quad (\text{A3})$$

The spatial wave functions and bare mass M_0 are obtained by solving the Schrödinger equation numerically using the Numerov method [35]. The full bare-mass spectrum is given in Ref. [12].

APPENDIX B: DETAILS OF THE COUPLED-CHANNEL EFFECTS

As sketched by Fig. 1, the experimentally observed state should be a mixture of the pure quarkonium state (bare state) and B meson continuum. The coupled-channel effects can be deduced by using

$$H_0|\psi_0\rangle = M_0|\psi_0\rangle \quad (\text{B1})$$

$$H_0|BC; p\rangle = 0 \quad (\text{B2})$$

$$H_{BC}|\psi_0\rangle = 0 \quad (\text{B3})$$

$$H_{BC}|BC; p\rangle = E_{BC}|BC; p\rangle \quad (\text{B4})$$

$$H|A\rangle = M|A\rangle, \quad (\text{B5})$$

where M_0 is the bare mass of the bottomonium and can be solved directly from the Schrödinger equation and M is the physical mass. The interaction between B mesons is neglected. When Eq. (B5) is projected onto each component, we immediately get

$$\langle\psi_0|H|\psi\rangle = c_0M = c_0M_0 + \int d^3p c_{BC}(p)\langle\psi_0|H_I|BC; p\rangle, \quad (\text{B6})$$

$$\langle BC; p|H|\psi\rangle = c_{BC}(p)M = c_{BC}(p)E_{BC} + c_0\langle BC; p|H_I|\psi_0\rangle. \quad (\text{B7})$$

Solving c_{BC} from Eq. (B7), substituting back to Eq. (B6), and eliminating the c_0 on both sides, we get an integral equation,

$$M = M_0 + \Delta M, \quad (\text{B8})$$

where ΔM is given in Eq. (5). Once M is solved, the coefficient of different components can be worked out too. For states below the threshold, the normalization condition $|A\rangle$ can be rewritten as

$$|c_0|^2 + \int d^3p |c_{BC}|^2 = 1. \quad (\text{B9})$$

After the substitution of c_{BC} , we get the probability of the $b\bar{b}$ component. The sum of BC is restricted to the ground-state $B_{(s)}$ mesons, i.e., $B\bar{B}, B\bar{B}^* + \text{H.c.}, B^*\bar{B}^*, B_s\bar{B}_s, B_s\bar{B}_s^* + \text{H.c.}, B_s^*\bar{B}_s^*$.

The coupled-channel effects calculation cannot proceed if the wave functions of the $|\psi_0\rangle$ and BC components are not settled in Eq. (7). Since the major part of the coupled-channel effects calculation is encoded in the wave function overlap integration,

$$\langle BC; p|H_I|\psi_0\rangle = \int d^3k \phi_0(\vec{k} + \vec{p}) \phi_B^*(\vec{k} + x\vec{p}) \phi_C^*(\vec{k} + x\vec{p}) \times |\vec{k}| Y_1^m(\theta_{\vec{k}}, \phi_{\vec{k}}), \quad (\text{B10})$$

where $x = m_q/(m_Q + m_q)$ and m_Q and m_q denote the bottom quark and the light-quark mass, respectively. The ϕ_0 , ϕ_B , and ϕ_C are the wave functions of $|\psi_0\rangle$ and BC components, respectively, and the notation $*$ stands for the complex conjugate. These wave functions are in momentum space, and they are obtained by the Fourier transformation of the eigenfunctions of the bare Hamiltonian H_0 . More details can be found in our earlier works [12,30].

APPENDIX C: HYPERFINE MASS SPLITTING FOR S-WAVE BOTTOMONIA

For the S -wave (η_b and Υ) bottomonia, we define

$$\delta M_S \equiv \frac{32\pi\alpha}{9m_b^2} |R(0)|^2. \quad (\text{C1})$$

Because of the $\mathbf{S} \cdot \mathbf{S}$ interaction term in Eq. (9), we have δM_0 :

$$\begin{aligned}\delta M_0(\eta_b) &= -\frac{3}{4}\delta M_S, \\ \delta M_0(\Upsilon) &= +\frac{1}{4}\delta M_S.\end{aligned}\quad (\text{C2})$$

After the suppression of $P_{b\bar{b}}(\eta_b)$ and $P_{b\bar{b}}(\Upsilon)$, the mass splitting becomes

$$\begin{aligned}M(\Upsilon) - M(\eta_b) &\equiv \delta M(\Upsilon) - \delta M(\eta_b) \\ &= \left(\frac{1}{4}P_{b\bar{b}}(\Upsilon) + \frac{3}{4}P_{b\bar{b}}(\eta_b)\right)\delta M_S.\end{aligned}\quad (\text{C3})$$

So for the S -wave bottomonium, we defined the weighted average of the $P_{b\bar{b}}$:

$$\tilde{P}_{b\bar{b}} = \frac{1}{4}P_{b\bar{b}}(\Upsilon) + \frac{3}{4}P_{b\bar{b}}(\eta_b).\quad (\text{C4})$$

-
- [1] A. M. Sirunyan *et al.* (CMS Collaboration), Observation of the $\chi_{b1}(3P)$ and $\chi_{b2}(3P)$ and Measurement of Their Masses, *Phys. Rev. Lett.* **121**, 092002 (2018).
- [2] G. Aad *et al.* (ATLAS Collaboration), Observation of a New χ_b State in Radiative Transitions to $\Upsilon(1S)$ and $\Upsilon(2S)$ at ATLAS, *Phys. Rev. Lett.* **108**, 152001 (2012).
- [3] R. Aaij *et al.* (LHCb Collaboration), Measurement of the $\chi_b(3P)$ mass and of the relative rate of $\chi_{b1}(1P)$ and $\chi_{b2}(1P)$ production, *J. High Energy Phys.* **10** (2014) 088.
- [4] R. Aaij *et al.* (LHCb Collaboration), Study of χ_b meson production in pp collisions at $\sqrt{s} = 7$ and 8 TeV and observation of the decay $\chi_b(3P) \rightarrow \Upsilon(3S)\gamma$, *Eur. Phys. J. C* **74**, 3092 (2014).
- [5] V. M. Abazov *et al.* (D0 Collaboration), Observation of a narrow mass state decaying into $\Upsilon(1S) + \gamma$ in $p\bar{p}$ collisions at $\sqrt{s} = 1.96$ TeV, *Phys. Rev. D* **86**, 031103 (2012).
- [6] K. Heikkilä, S. Ono, and N. A. Tornqvist, Heavy $c\bar{c}$ and $b\bar{b}$ quarkonium states and unitarity effects, *Phys. Rev. D* **29**, 110 (1984).
- [7] S. Ono and N. A. Tornqvist, Continuum mixing and coupled channel effects in $c\bar{c}$ and $b\bar{b}$ quarkonium, *Z. Phys. C* **23**, 59 (1984).
- [8] S. Ono, A. I. Sanda, N. A. Tornqvist, and J. Lee-Franzini, Where are the $B\bar{B}$ Mixing Effects Observable in the Υ Region? *Phys. Rev. Lett.* **55**, 2938 (1985).
- [9] S. Ono, A. I. Sanda, and N. A. Tornqvist, B meson production between the $\Upsilon(4S)$ and $\Upsilon(6S)$ and the possibility of detecting $B\bar{B}$ mixing, *Phys. Rev. D* **34**, 186 (1986).
- [10] I. K. Hammer, C. Hanhart, and A. V. Nefediev, Remarks on meson loop effects on quark models, *Eur. Phys. J. A* **52**, 330 (2016).
- [11] L. Micu, Decay rates of meson resonances in a quark model, *Nucl. Phys. B* **10**, 521 (1969).
- [12] Y. Lu, M. N. Anwar, and B. S. Zou, Coupled-channel effects for the Bottomonium with realistic wave functions, *Phys. Rev. D* **94**, 034021 (2016).
- [13] J. Ferretti and E. Santopinto, Higher mass bottomonia, *Phys. Rev. D* **90**, 094022 (2014); Quark structure of the $X(3872)$ and $\chi_b(3P)$ resonances, *Phys. Rev. D* **90**, 054010 (2014); Threshold corrections of $\chi_c(2P)$ and $\chi_b(3P)$ states and $J/\psi\rho$ and $J/\psi\omega$ transitions of the $X(3872)$ in a coupled-channel model, *Phys. Lett. B* **789**, 550 (2019).
- [14] C. O. Dib and N. Neill, $\chi_b(3P)$ splitting predictions in potential models, *Phys. Rev. D* **86**, 094011 (2012).
- [15] Y. Lu, M. N. Anwar, and B. S. Zou, How large is the contribution of excited mesons in coupled-channel effects?, *Phys. Rev. D* **95**, 034018 (2017).
- [16] S. Godfrey and K. Moats, Bottomonium mesons and strategies for their observation, *Phys. Rev. D* **92**, 054034 (2015).
- [17] J. Z. Wang, Z. F. Sun, X. Liu, and T. Matsuki, Higher bottomonium zoo, *Eur. Phys. J. C* **78**, 915 (2018).
- [18] J. Segovia, P. G. Ortega, D. R. Entem, and F. Fernandez, Bottomonium spectrum revisited, *Phys. Rev. D* **93**, 074027 (2016).
- [19] T. J. Burns, How the small hyperfine splitting of P-wave mesons evades large loop corrections, *Phys. Rev. D* **84**, 034021 (2011); P-wave spin-spin splitting and meson loops, arXiv:1108.5259.
- [20] T. Barnes, S. Godfrey, and E. S. Swanson, Higher charmonia, *Phys. Rev. D* **72**, 054026 (2005).
- [21] C. Patrignani *et al.* (Particle Data Group), Review of particle physics, *Chin. Phys. C* **40**, 100001 (2016).
- [22] E. Hiyama, Y. Kino, and M. Kamimura, Gaussian expansion method for few-body systems, *Prog. Part. Nucl. Phys.* **51**, 223 (2003).
- [23] R. F. Lebed and E. S. Swanson, Quarkonium h states as arbiters of exoticy, *Phys. Rev. D* **96**, 056015 (2017).
- [24] R. F. Lebed and E. S. Swanson, Heavy-quark hybrid mass splittings: Hyperfine and “ultrafine,” *Few-Body Syst.* **59**, 53 (2018).
- [25] Y. Kiyo and Y. Sumino, Full formula for heavy quarkonium energy levels at next-to-next-to-next-to-leading order, *Nucl. Phys. B* **889**, 156 (2014); Perturbative heavy quarkonium spectrum at next-to-next-to-next-to-leading order, *Phys. Lett. B* **730**, 76 (2014).
- [26] W. E. Caswell and G. P. Lepage, Effective Lagrangians for bound state problems in QED, QCD, and other field theories, *Phys. Lett. B* **167B**, 437 (1986).
- [27] N. Brambilla, A. Pineda, J. Soto, and A. Vairo, Potential NRQCD: An effective theory for heavy quarkonium, *Nucl. Phys. B* **566**, 275 (2000).
- [28] W. Kwong and J. L. Rosner, D wave quarkonium levels of the Υ family, *Phys. Rev. D* **38**, 279 (1988).
- [29] B. Q. Li and K. T. Chao, Bottomonium spectrum with screened potential, *Commun. Theor. Phys.* **52**, 653 (2009).

- [30] Y. Lu, M. N. Anwar, and B. S. Zou, $X(4260)$ revisited: A coupled channel perspective, *Phys. Rev. D* **96**, 114022 (2017).
- [31] Y. S. Kalashnikova, Coupled-channel model for charmonium levels and an option for $X(3872)$, *Phys. Rev. D* **72**, 034010 (2005).
- [32] E. Eichten, K. Gottfried, T. Kinoshita, K. D. Lane, and T. M. Yan, Charmonium: The model, *Phys. Rev. D* **17**, 3090 (1978); *Phys. Rev. D* Erratum **21**, 313(E) (1980).
- [33] E. Eichten, K. Gottfried, T. Kinoshita, K. D. Lane, and T. M. Yan, Charmonium: Comparison with experiment, *Phys. Rev. D* **21**, 203 (1980).
- [34] B. Q. Li, C. Meng, and K. T. Chao, Coupled-channel and screening effects in charmonium spectrum, *Phys. Rev. D* **80**, 014012 (2009).
- [35] B. Numerov, Note on the numerical integration of $d^2x/dt^2 = f(x, t)$, *Astron. Nachr.* **230**, 359 (1927).